ACS OMEGA

Article

Cite This: ACS Omega 2019, 4, 9407−9418

http://pubs.acs.org/journal/acsodf

Control of Functionalities in GO: Effect of Bronsted Acids as Supported by Ab Initio Simulations and Experiments

Nisha Yadav,[†] Vedha Kallur,[†] Dwaipayan Chakraborty,[‡] Priya Johari,*[,‡] and Bimlesh Lochab*[,†]

[†]Materials Chemistry Laboratory, Department of Chemistry, School of Natural Sciences, and [‡]Computational Materials Physics Laboratory, Department of Physics, School of Natural Sciences, Shiv Nadar University, Gautam Buddha Nagar, Greater Noida, Uttar Pradesh 201314, India

Supporting Information

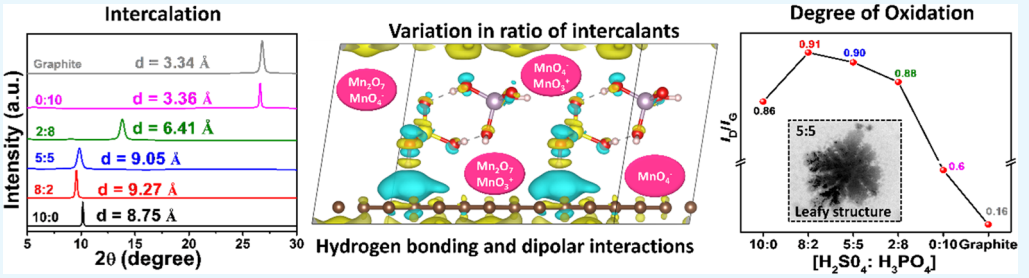

ABSTRACT: Graphene oxide (GO) is an attractive precursor for graphene, provided by the well-known wet-chemical oxidative process. The intercalation of acid in graphite is considered as a crucial step, and its subsequent oxidation holds special relevance in synthesis. So far, the above chemistry is dominated by usage of H_2SO_4. Recently, H_3PO_4 appeared as a suitable intercalant for graphite. However, its role is not well understood in the formation of GO, especially when present as a co-acid with H_2SO_4. Additionally, a relatively lower toxicity of H_3PO_4 as compared to H_2SO_4, elimination of toxic $NaNO_3$ usage, and a facile purification protocol are encouraging in terms of low-cost production of GO with a reduced environmental impact. Here, we report the systematic synthesis and characterization of GOs prepared with the variation in the ratio of H_2SO_4 and H_3PO_4. Ab initio simulations revealed that intercalation is primarily affected because of the usage of a mixture of co-acids. Interestingly, the ratio of the acids dictated the nature of the functionalities, extent of the defects, and morphology of the GOs, accounting for a pronounced effect on thermal stability, contact angle, zeta potential, and hydrodynamic size. The oxidation mechanism showed a predominance of H_2SO_4 content, whereas H_3PO_4 is found to mainly govern the intercalation of graphite, thereby affecting the acid-based intercalation−oxidation chemistry of graphite. The as-prepared GO suspension exhibited a high adsorption capacity for methylene blue dye removal in water, suggesting its potential as an adsorbent material in water treatment. The utility of the two acids affects the acid-based intercalation−oxidation chemistry of graphite and simultaneously may open up new opportunities for synthesized GOs, on tenets of green chemistry, in a wide arena of applications.

1. INTRODUCTION

Graphene oxide (GO) acts as a suitable precursor of graphene because of its relative ease of preparation, handling, and processability at a lower cost, thereby enabling its commercial applicability. It can be used as such or modified chemically and/or thermally to further extend its utility. Electronic and electrical applications demand a more intact carbon framework of graphene with a larger sheet size and existence of functionalities on the edges, whereas biomedical applications favor a smaller sheet size with a higher degree of functionalities at both edges and the basal plane. Thus, a good control in sheet size, oxygen content, and nature of functionalities with optimization of the synthesis process is of paramount importance to dictate the end-use application.

In general, the wet-chemical oxidative synthetic route for interconversion of graphite to GO involves four steps,[1] namely, (a) graphite intercalation, (b) oxidation, (c) exfoliation of oxidized sheets, and (d) subsequent purification to remove impurities. The extent of oxidation and nature of functionalities in GO is affected by the nature and source of graphite,[2,3] amount,[4,5] and nature of oxidant,[6,7] water,[8] hydrogen peroxide,[9] sulfuric acid, physical parameters such as temperature,[10] and reaction time.[11−13]

The formation of graphite intercalation compounds (GICs) involves insertion of small molecules/ions (guest) within the layers of graphite (host) as favored by effective host−guest energetic dynamics and interaction.[14−18] Schafhaeutl and Brodie noticed the appearance of "blue-lustrous color" in reflected and "purple color" in transmitted light because of reaction of graphite with H_2SO_4 and oxidizing agents, which are attributed to the formation of GICs.[19,20] Hofmann and Thiele reported the formation of GICs with H_2SO_4, in the

Received: March 11, 2019
Accepted: May 16, 2019
Published: May 29, 2019

DOI: 10.1021/acsomega.9b00676
ACS Omega 2019, 4, 9407−9418

presence of HNO_3, $KMnO_4$, HIO_4, $HClO_4$, selenic acid, and phosphoric acid.[21,22] The so-formed GICs are highly unstable and known to decompose instantaneously even with atmospheric moisture. It is reported that the oxidation of graphite to form C−O bonds occurs at the intercalation stage and/or with the treatment of $KMnO_4$, as aided by the generation of charge on the sp^2-hybridized carbon.[23] The interlayer distances of GICs formed by H_2SO_4 and H_3PO_4 are similar, 7.3−7.9 Å, with the latter having a higher intercalation efficiency, suggesting that H_3PO_4 is as equally effective as H_2SO_4 and worth exploring in graphene chemistry.[24]

Exfoliation of graphite flakes into defect-free few-layer graphene via a nonoxidative route is also reported by forming GICs[24,25] and then explored for various applications.[26,27] Recently, graphite intercalation has also been mediated by a K−tetrahydrofuran complex, which facilitates the diffusion of DMSO molecules into the intergalleries and results in widening of the interlayer spacing by inducing strong dipolar interactions.[28] However, all these reports are limited to exfoliation without proceeding further to the oxidation step.

Nishina et al.[29] reported that $KMnO_4$ and H_2SO_4 alone are sufficient to convert graphite to GO and $NaNO_3$ is not necessary to facilitate oxidation. Similarly, Tour et al.[30] eliminated the utility of $NaNO_3$ by the introduction of H_3PO_4 as a co-acid to H_2SO_4 (1:9, v/v) in $KMnO_4$ (six equivalents)-mediated oxidation of graphite. Lochab et al.[31] further simplified the purification procedure of GO synthesized by an improved method. GO synthesized by the improved method differs significantly from Hummers' method and revealed a predominance of different types of oxidative functionalities, suggesting the role of H_3PO_4 in affecting the extent of oxidation. Likewise, H_3PO_4 and H_3BO_3 also assisted in a reasonable exfoliation of graphite.[32] Recently, efficacies of intercalants on graphite have regenerated research interest, and it is worth exploring their potential in generation of oxidized graphene materials. However, the subsequent role of intercalation during the oxidation of graphite to form GO still demands further exploration. Interestingly, the greener aspect in GO preparation by recycling and reuse of sulfuric acid is found to be attractive as it reduced the amount of water required for purification and thereby lowered the overall production cost.[33] Kumar and Srivastava et al.[34] reported electrochemical exfoliation of graphite electrodes in the presence of H_2SO_4 and H_3PO_4 as a pretreatment step, followed by oxidation as a simple synthetic route for preparation of ∼10 μm GO sheets.

The most widely used Hummers' method for synthesis of GO involved treatment of graphite with $KMnO_4$ and $NaNO_3$ in concentrated H_2SO_4 at 98 °C. The reaction is considered to be hazardous, especially during the scale-up of the reaction. Furthermore, the requirement of higher volumes of acids demands an excessive amount of water for purification to alleviate the corrosive nature of nanoparticles.[35] This process accounts to a higher E-factor (environmental) with generation of more waste, as a consequence leading to a greater negative environmental impact. This motivates exploration of an effective substitute to H_2SO_4 and $NaNO_3$, which can add greener potential to widely synthesized GO nanomaterial.

Interestingly, H_3PO_4 is a weak acid with relatively lower toxicity and without hazardous issues of gas liberation. It is widely used as a food additive and as an acidifying additive in soft drinks. In the current work, GO is synthesized using various co-mixtures of H_2SO_4 and H_3PO_4 (v/v) to analyze the effect of addition of H_3PO_4 on GO properties. Figure 1 shows a generalized synthetic procedure adopted in the current work,

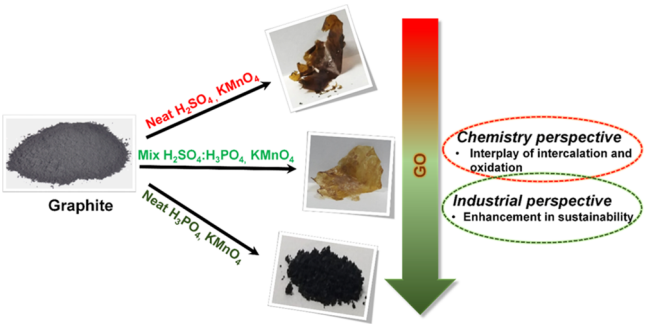

Figure 1. Schematic illustration of intercalation and oxidation chemistry of graphite using acids.

and it is considered to be sustainable as compared to Hummers' method because of the following reasons: (i) H_2SO_4 is a highly corrosive irritant with a very high toxicological profile, raising environment concerns, and therefore, a safer alternative, H_3PO_4, with equivalent intercalating efficacy in graphite needs exploration; (ii) no generation of the toxic gas(es) SO_x and NO_x because of reduction in the volume of H_2SO_4 usage and elimination of $NaNO_3$ in the process, respectively; (iii) reaction is carried out at a milder temperature of 50 °C, preventing explosion due to in situ generated oxidant Mn_2O_7 from $KMnO_4$ in acidic medium;[36] (iv) lower energy requirement for the reaction; and (v) purification of synthesized GOs is followed mainly by a simple gravity-settling process to encourage bulk synthesis with a cost-effective and time-saving protocol.

To further understand the role of acid intercalants on graphite, we also performed computational studies. Experimentally, GOs are analyzed systematically to determine the nature and extent of oxygen-rich functionalities with variation in the ratio of intercalants. An appreciable effect in generated oxo-functionalities in GOs is revealed as a function of the acid ratio, simultaneously assisting in developing an understanding of acid-based intercalation−oxidation chemistry of graphite. The so-formed GOs differ significantly in their properties, which may open up new avenues to various graphene-dominated applications.

2. EXPERIMENTAL SECTION

2.1. Materials. Graphite flakes (Alfa Aesar, 99.8%, 325 mesh, 44 μm), sulfuric acid (Finar), potassium permanganate, phosphoric acid, hydrogen peroxide (30%, w/v), and methylene blue (MB) dye (Fisher Scientific) were used as received.

2.2. Characterization Techniques. Fourier transform infrared (FT-IR) spectra were recorded on a Nicolet iS5 spectrometer equipped with an iD5-ATR accessory, in the range of 800−2000 cm^{-1} with a resolution of 4 cm^{-1}. Absorbance measurements were carried out on a Thermo Scientific Evolution 201 UV−vis spectrophotometer by preparing dispersions of the respective nanomaterial in deionized water. Raman spectra were obtained using a STR 500 confocal micro-Raman spectrometer by Airix Corporation at λ of 532 nm. The distance between defects points (L_D) and average crystallite size (L_a) of the sp^2 domains in the GO samples was calculated according to the literature.[37,38] X-ray

DOI: 10.1021/acsomega.9b00676
ACS Omega 2019, 4, 9407−9418

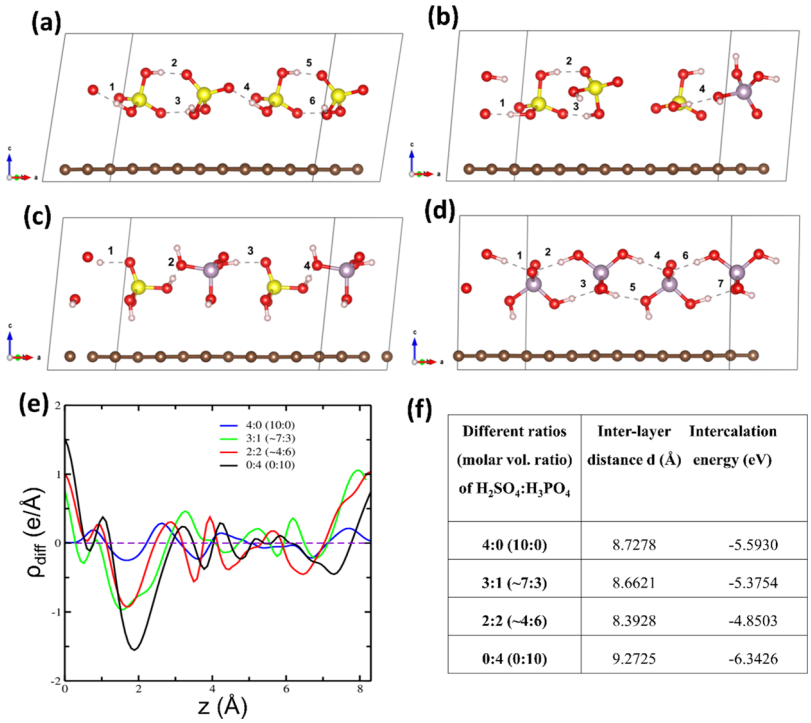

(f)

Different ratios (molar vol. ratio) of H_2SO_4:H_3PO_4	Inter-layer distance d (Å)	Intercalation energy (eV)
4:0 (10:0)	8.7278	-5.5930
3:1 (~7:3)	8.6621	-5.3754
2:2 (~4:6)	8.3928	-4.8503
0:4 (0:10)	9.2725	-6.3426

Figure 2. Optimized lowest energy structures in each ratio (molar volume ratio) (a) 4:0 (10:0), (b) 3:1 (~7:3), (c) 2:2 (~4:6), and (d) 0:4 (0:10) of H_2SO_4 and H_3PO_4. Dashed lines show hydrogen bonding. Yellow, purple, red, white, and brown balls denote sulfur, phosphorus, oxygen, hydrogen, and carbon atoms, respectively. (e) 1D differential charge density plot of graphite intercalated with H_2SO_4 and H_3PO_4 in each ratio. (f) Table 1: Interlayer distance and intercalation energy for different ratios of H_2SO_4 and H_3PO_4.

diffraction (XRD) studies were performed on PANalytical X'pert Pro Powder with Cu Kα radiation (λ = 1.5406 Å). X-ray photoelectron spectroscopy (XPS, Omicron Multiprobe Surface Analysis System) measurements were carried out using a monochromatized Al Kα (1486.7 eV) radiation source to analyze the surface chemistry of synthesized GOs. Thermal behavior was investigated using Shimadzu, Japan, DTG-60 in the temperature range of 50−800 °C under nitrogen atmosphere at a heating rate of 10 °C/min. Elemental analysis was performed using Elementar (Germany, Vario EL III). The average particle size and zeta potential (ζ) of the particles were measured by the dynamic light scattering (DLS) instrument (Nanosizer, Malvern, UK) with an Ar laser (λ = 830 nm, detector angle = 90°, and sample volume = 10 μL at room temperature). The surface morphology of synthesized GOs was studied using scanning electron microscopy (SEM; Nova Nano FE-SEM 450 (FEI)) and transmission electron microscopy (TEM; The Tecnai G2 20 (FEI) S-Twin) at an accelerating voltage of 10 and 200 kV, respectively. Contact angle (CA) measurements were performed to characterize the surface properties of GO on glass substrates using a CA Metering System ACAM D3 (Apex Instruments). A drop of MilliQ water (2 μL) was placed on the surface of the GO-coated surface (200 μL of GO dispersion, 0.5 mg/mL followed by heating in an air-oven at 50 °C), and images were immediately captured using a CCD camera equipped with a magnifying lens. The CA reported is an average value of five measurements at different locations. The optical images of GO coated on the glass substrate were taken using a fluorescence microscope (Nikon, eclipse Ti-U, Make-Japan). For dye removal assay, GO (1.5 mg/mL, 400 μL) was mixed with MB (1 mg/L, 800 μL) by a vortex mixer. The suspension was incubated at 25 °C for 1 h and then centrifuged (Eppendorf 5810R) at 14 000 rpm for 20 min, and a supernatant was used to record the absorbance.

2.3. Computational Details. The computational study of intercalation of H_2SO_4 and H_3PO_4 acids between the graphitic layers was performed using the density functional theory-based approach, as implemented in the Vienna Ab initio Simulation Package (VASP).[39,40] A 6 × 3 × 1 supercell of graphite was considered to model GIC with different concentrations of acid molecules having H_2SO_4/H_3PO_4 ratios (with molar volumetric ratios in parenthesis) as 4:0 (10:0), 3:1 (~7:3), 2:2 (~4:6), and 0:4 (0:10) in between the carbon layers. For each ratio, various configurations of GIC were modeled and relaxed to obtain the minimum energy structure. The electron−ion interactions in all the calculations were treated using projector-augmented wave[41] pseudo-potentials with a plane-wave energy cutoff of 520 eV. To account for the exchange correlation interactions, the generalized gradient approximation with van der Waals (vdW) corrections [optimized Perdew−Burke−Ernzerhof-vdW (optPBE-vdW)][42−45] was used to incorporate vdW interactions between the acid molecules and the graphitic layers. A Γ-centered k-point grid of 4 × 8 × 4 was considered for all the abovementioned configurations. The total energy convergence criterion for the self-consistent calculations was set to be 10^{-4} eV, whereas a Hellmann−Feynman force convergence criterion of 0.01 eV/Å was set for all the calculations.

2.4. Oxidation of Graphite. To graphite flakes (0.5 g) in a conical flask kept in an ice bath, a designated volume of the H_2SO_4/H_3PO_4 (67 mL; 10:0, 8:2, 5:5, 2:8, 0:10, v/v) mixture was added. The mixture was stirred for 15 min before the addition of $KMnO_4$ (3 g). Upon complete addition, the reaction mixture was heated to 50 °C and stirred for 12 h. The reaction was allowed to cool down to room temperature before

DOI: 10.1021/acsomega.9b00676
ACS Omega 2019, 4, 9407−9418

addition of H_2O_2 (3 mL) followed by the addition of distilled water (220 mL). The reaction mixture was allowed to stir for 15 min, and the stirring was stopped to carry out the purification process. Purification was carried out by gravity settling for ratios 10:0, 8:2, and 5:5 and the rest were purified by centrifugation. The residue of GO was washed and re-dispersed in water to remove excess acid until the pH of the supernatant was found to be neutral. The residue obtained was dried at 60 °C in a vacuum oven to form GO. The GOs synthesized are named as 10:0, 8:2, 5:5, 2:8, and 0:10 depending on the ratio of H_2SO_4/H_3PO_4 used in the synthesis.

3. RESULTS AND DISCUSSION

The formation of GICs occurs via protonation of the benzenoid ring with acid to form graphite sulfuric acid intercalate, $[C_{24}^{+}(HSO_4^{-})(H_2SO_4)_2]_n$,[21] with an increase in interlayer spacing to 7.98 Å (cf. graphite 3.4 Å).[1,46] Likewise, H_3PO_4 also accounted for the expansion of graphite layers.[24] At this stage, a fewer lattice defects are also generated because of formation of oxo-species[47,48] on H_2SO_4-intercalated graphene as a result of electron transfer to the conducting graphite with compensation of charges prior to the entry of $KMnO_4$.[49] This suggested intercalation as one of the crucial steps, and it may be responsible for affecting the quality of oxidized graphene.[50] The intercalants act by opening up the edge of graphite, allowing the diffusion of acid further to open the gap in the graphite sheets. Once entered, it impedes the re-stacking of the sheets, mediating the entry of oxidizing agents and assisting their oxidation. The most widely used acid is H_2SO_4, which acts as an intercalant and also provides acidic pH to assist in the oxidation of graphite with $KMnO_4$.

Therefore, it is crucial to understand the effect of intercalants on the interlayer spacing in graphite and on the associated intercalation energy. First-principles quantum chemical calculations are performed to model the graphitic systems with intercalant acid molecules H_2SO_4/H_3PO_4 in the ratios of 4:0 (10:0), 3:1 (7:3), 2:2 (4:6), and 0:4 (0:10) with the molar volumetric ratio given in parenthesis. Figure 2a–d depicts the optimized structure of the lowest energy configurations for each ratio of H_2SO_4/H_3PO_4. The formation of hydrogen bonding in between the acid molecules is clearly evident from Figure 2, confirming their dipole–dipole intermolecular interactions. The distances between oxygen and hydrogen atoms participating in hydrogen bonding are summarized in Table S1. It can be noticed from the table that a short intermolecular oxygen–hydrogen bond forms in between the two H_2SO_4 acid molecules, as can be seen in the cases of 4:0 and 3:1 (where the concentration of H_2SO_4 is higher). However, with the increase in H_3PO_4 content, longer bonding interactions are observed.

Table 1 (in Figure 2) tabulates the interlayer distance between the graphene layers that changes because of intercalation of acid molecules. On analyzing the data, we noticed that the interlayer distance is maximum (9.27 Å) in the case of neat H_3PO_4 (0:10), followed by neat H_2SO_4 (8.73 Å), confirming that H_3PO_4 is as equally effective as H_2SO_4 in expanding the graphitic galleries, well in agreement with the results of Kovtyukhova et al.[24] In the case of mixed acid concentrations, however, a relative decrease in the interlayer distance is noticed. This distance decreases with the addition of H_3PO_4 and goes to 8.66 Å and then 8.39 Å, when the H_2SO_4/H_3PO_4 ratio is 3:1 (~7:3) and 2:2 (~4:6), respectively. To check the variation of the intercalation efficiency with respect to the acid ratio, we calculated the intercalation energy, as shown in Table 1. Interestingly, a similar trend to the interlayer distance is noticed in the intercalation energy. The value is maximum in the case of neat H_3PO_4, 0:10 (−6.34 eV), whereas minimum is observed in the 4:6 ratio (−4.85 eV). Overall, the intercalation energy is found to decrease with the increase in the concentration of H_3PO_4 in the acid mixture. These results suggest that the highest intercalation efficiency for H_3PO_4 may provide enhancement in the formation of GIC.

To understand these results in depth and further validate our claim, the charge density difference ($\rho_{diff} = \rho_{graphene+mols} - \rho_{graphene} - \rho_{mols}$) is calculated. The charge density differences in 1-D and 3-D for each of the four computationally investigated systems are depicted in Figures 2e and S1, respectively. The formation of dipoles in between graphene and the molecules is clearly evident from Figure S1. It is noticed that the maximum charge transfer takes place in the interface region between the graphene sheet and the acid molecules. Dipoles are also found to form around the molecules (when z = 1.5–2 Å) where H_3PO_4 is present. Interestingly, except in case of neat H_2SO_4, the dipole strength is found to be maximum near the graphene sheets only. Thus, as compared to H_2SO_4 molecules, H_3PO_4 acid molecules are found to transfer more charge to the graphene sheet, as shown in Figure S1, suggesting that H_3PO_4 molecules may provide assistance for charge transfer to graphene through dipole formation.

The computational results suggest that the incorporation of H_3PO_4 molecules can be helpful to increase the intercalation efficiency of graphite layers. The formation of hydrogen bonding in between the acid molecules can further assist the chemical oxidation process at the basal plane efficiently. Therefore, based on our computational intercalation efficiency results of the acid mixture combination, the experiments were performed by varying the ratio of acids (H_2SO_4 and H_3PO_4) systematically to mediate the synthesis of GO with $KMnO_4$ and to unravel their effect on the properties of GO.

As graphite oxidation is also facilitated by water and hydrogen peroxide,[8,51−54] the same quantity of both is utilized to assist the comparison. To begin with, the effect of variation on the acid ratio is monitored during synthetic steps and the respective yields of GO are obtained, as shown in Figure 3 and Table S2.

The usual purple color of $KMnO_4$ is observed in graphite initially. The addition of acid (nature and ratio) to the reaction mixture resulted in noticeable color changes with time (0.5 h vs 12 h), as shown in Figure 3b. Neat H_2SO_4 addition showed a characteristic green color. With an increase in H_3PO_4 in the acid ratio, a drastic color change is observed. In the initial 30 min, H_2SO_4/H_3PO_4 samples showed a greenish to reddish brown, and then further pink and black colors after 12 h, suggesting the effect of variation in the ratios of the two acids in the formation of GO. Further, the addition of hydrogen peroxide/water also resulted in a visible change in color from the usual yellowish-orange to lustrous black with increase in the amount of H_3PO_4 in the reaction mixture.

The appearance of different colors at various stages is a consequence of subsequent intercalation/de-intercalation of compounds and existence of different oxidation states of manganese ions in the reaction mixture. In general, bulk synthesis of GO is indicated by the conversion of black color of graphite to yellow color in aqueous peroxide, which upon drying resulted in the formation of a brown to yellow graphite

DOI: 10.1021/acsomega.9b00676
ACS Omega 2019, 4, 9407−9418

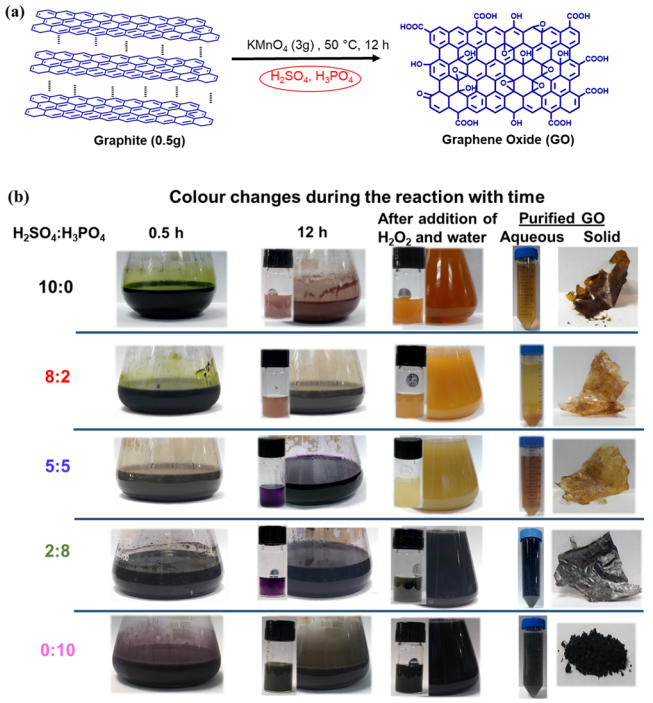

Figure 3. (a) Synthetic scheme for GO preparation; (b) optical images during synthesis of GO with variation of the intercalant ratio (H_2SO_4/H_3PO_4) at various stages captured at different times. The inset shows the diluted volumes of the reaction mixture which can be noticed by the respective color changes.

oxide. In our case, the finally purified GO showed both a different color and state. The 10:0 ratio resulted in a brown film, whereas 0:10 existed as a black lustrous powder. The intermediate ratios exhibited a lighter shade of brown and yellow thin films, whereas 8:2 resulted in a black film. Furthermore, the yield of the obtained oxidized material is varied and is found to be substantially high when H_3PO_4 is present as a co-acid in the reaction mixture. A higher yield is suggestive of the formation of a highly oxidized material[26] and entrapment of species, if any.

The effect of different intercalating agents on conversion of graphite to oxidized material is analyzed by XRD, as shown in Figure 4a. It is reported that besides the reaction conditions, the temperature of drying of GO dispersion is also important,[12] which is again kept the same, to ascertain and compare the degree of oxidation in synthesized GO by XRD. The absence of the characteristic peak due to graphite at 26.8° excludes their occurrence in all the samples except 0:10 in H_2SO_4/H_3PO_4. The interlayer spacing (d) evaluated on the d_{001} plane can be correlated to the degree of oxidation. The "d" value between the layers increased from 3.35 Å in pristine graphite to 8.75 Å in neat H_2SO_4 (10:0)-treated graphite and is found to be in excellent agreement with our computational analysis (8.73 Å in H_2SO_4-intercalated graphite, Table 1). On the contrary, neat H_3PO_4 (0:10) revealed a "d" value of 3.36 Å, suggesting that H_2SO_4 may have a higher potential to assist exfoliation and oxidation of graphite than H_3PO_4 alone. However, the former option may be ruled out, as H_3PO_4 exhibited a higher interlayer distance, intercalation energy, and charge density accumulation in graphene sheets as observed from our computational studies.[24] Additionally, this is also supported from our observation that with the addition of H_3PO_4 in H_2SO_4, that is, when the acid ratio (H_2SO_4/H_3PO_4) is 8:2, the highest evaluated "d" of 9.27 Å was revealed, representing the strongest oxidation and higher exfoliation. A lower "d" of 9.0 Å is reported with the 9:1 (H_2SO_4/H_3PO_4) mixture for the same size graphite flakes.[30] This further confirmed that an initial increase in H_3PO_4 content in H_2SO_4 assisted in expanding the graphite galleries to aid the oxidation of basal planes. With further increase in H_3PO_4 content, that is, 5:5 and 2:8, "d" reduced to 9.05 and 6.41 Å, respectively, supporting a lowering in the capability of the acid mixture to facilitate oxidation of graphite by $KMnO_4$. The XRD results suggested that oxidation is extensive up to an equal volume ratio (5:5) of the acids.

A similar reduction in the interlayer distance is observed in the co-acid mixture from our computational results, as shown in Table 1. The primary step for the formation of GICs involved protonation of the benzene ring with acid followed by reactions facilitating the generation of oxo-functionalities in graphite. Therefore, H_3PO_4 may be prudential to form GIC, but may not be as effective as H_2SO_4 to oxidize because of its relatively weak acidic nature, as apparent from its acidity dissociation constant (K_a) values, H_2SO_4 (1.1×10^3) $\gg$ H_3PO_4 (7.1×10^{-3}). Probably, an optimum ratio of two acids is desired to facilitate both exfoliation and oxidation. It is well known that $KMnO_4$ exhibits variable oxidation states depending upon the nature and pH of the mixture. Neat H_3PO_4 and up to 50% of H_3PO_4 conc. showed a reduction in the oxidation state of manganese in $KMnO_4$ from Mn^{7+} to Mn^{3+} with an in situ evolution of oxygen.[55] However, in neat H_2SO_4, it changes from Mn^{7+} to Mn^{2+}, indicating different oxidizing potentials of permanganate in the presence of two acids.

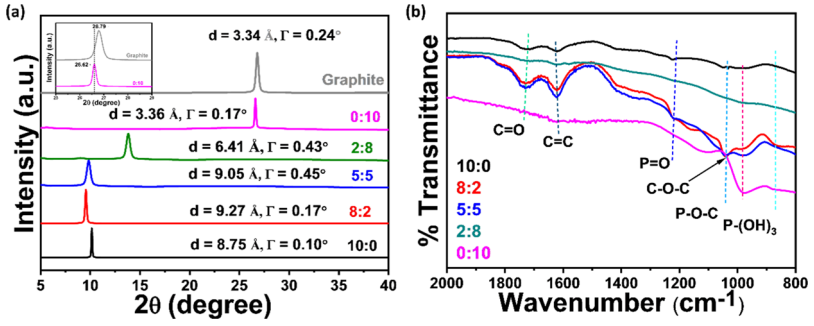

Figure 4. (a) Powder XRD spectra of graphite and GOs synthesized by varying intercalant ratios (H_2SO_4/H_3PO_4) with their corresponding interlayer spacing "d" (calculated using Bragg's equation: $n\lambda = 2d \sin\theta$) and fwhm (Γ) values. (b) FTIR spectra of synthesized GOs and their characteristic vibration bands due to presence of different oxygenated functionalities.

DOI: 10.1021/acsomega.9b00676
ACS Omega 2019, 4, 9407−9418

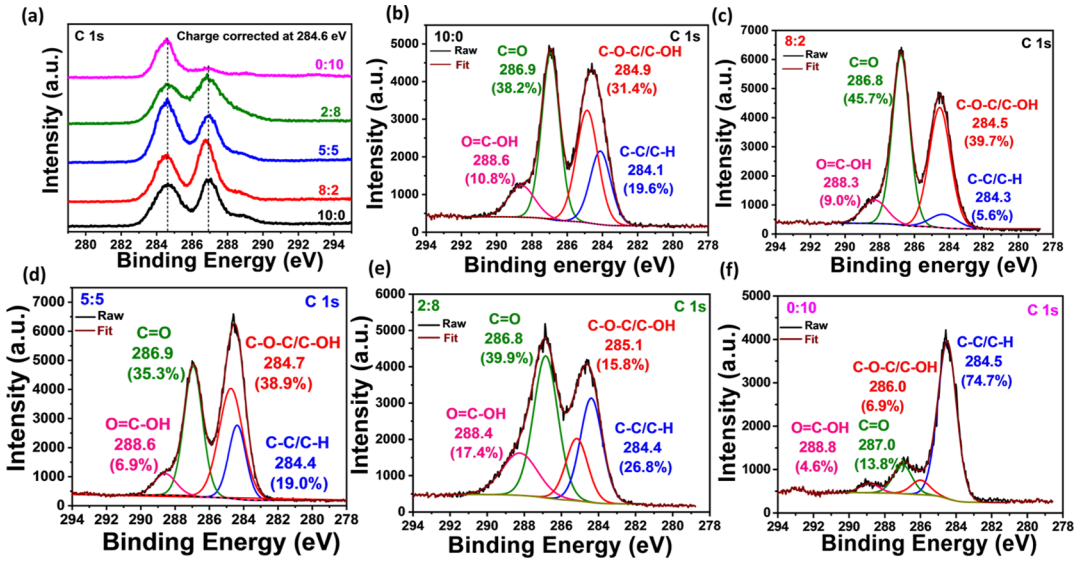

Figure 5. High-resolution XPS spectra: (a) stacked C 1s; (b–f) deconvoluted C 1s of synthesized GOs with variation in the extent and nature of oxidative functionalities. The four distinct regimes observed are COOH (pink), C═O (green), C−O−C/C−OH (red), and C═C, C−C, C−H (blue).

Additionally, a significant broadening in the XRD peak in synthesized GOs is observed as confirmed from the change in the full width at half maximum (fwhm, Γ) from 0.1 to 0.4 in 10:0 to 2:8 of H_2SO_4/H_3PO_4-treated graphite, as shown in Figure 4a. This is attributed to the lattice distortion that occurs in the vertical stacking order of the graphite lattice[56] because of the generation of heterogeneous nanostructures associated with variable extents of oxidation. As compared to graphite, the 0:10 sample (inset of Figure 4a) clearly showed a substantial difference in Γ and peak position. This shift to a lower 2-theta value and reduced Γ in 0:10 can be attributed to the changes in the chemical/physical environment across the sheets upon treatment with H_3PO_4.

Chemical oxidation of graphite to GO is supported by FTIR (Figure 4b) and is consistent with the literature data.[57] The characteristic stretching vibration modes due to O−H, >C═O of carboxylic acid and ketonic, sp^2-hybridized C═C, and C−O−C epoxide functionalities are observed at 3200, 1730, 1625, and 1054 cm^{-1}, respectively.[58,59] As compared to 10:0, the prominence of >C═O, C−O−C, and the O−H peak in ratios 8:2 and 5:5 is apparent, confirming the richness of their surfaces with highly oxidized functionalities. In the case of 2:8 and 0:10, the peaks are ill-defined and quite broad. This suggested the occurrence of either a comparative lower degree of oxidation and/or existence of physically and chemically bound structures due to H_3PO_4 treatment on graphite, which is in congruence with XRD. The 0:10 sample showed intense stretching vibrations because of H_3PO_4 and organo-phosphates. The peaks observed at 980, 1178, and 890 cm^{-1} are attributed to the P−O−C, hydrogen-bonded P═O, and P−O bond, respectively.[60,61]

Figure 5 shows the XPS of GOs to understand the effect of addition of H_3PO_4 as a co-acid on the generation of chemical functionalities in GO. A significant difference in the C 1s XPS spectra (Figure 5a) is reflected, confirming the potentiality in the formation of different types of oxidative-functionalized species on the surface of GO by varying the ratio of the two acids. The C 1s XPS spectra of all the synthesized GOs (Figure 5b–f) are de-convoluted and fitted at a binding energy (B.E.) of ∼284.6, 286.2, 288.1, and 289.6 eV corresponding to the C═C/C−C/C−H, C−OH/epoxy, C═O, and COOH functional groups, respectively. The evolution of various functionalities and their respective percentage components determined are tabulated in Table S3.

In general, epoxy and hydroxyl functionalities exist on the basal plane, and their further oxidation demands breaking of C−C bonds to introduce ketones and further to carboxyl functionalities that are located at the edges of basal planes or at the periphery of GO.[62] As the source of graphite and the adopted methodology are similar, the formation of various oxidized functionalities is mainly attributed to the variation in the acid ratio. The 10:0 and 0:10 samples clearly showed that neat H_2SO_4 resulted in the formation of a relatively higher oxidized surface as compared to neat H_3PO_4 (Figure 4b), which is in accordance with their effect on the oxidizing potential of $KMnO_4$ and intercalation efficiency of graphite.[24,55]

It is observed that H_3PO_4 is not as effective as H_2SO_4 to enable the oxidation of carbonyl groups further to carboxylic acid. The peak corresponding to nonoxidized graphitic C−C bonds at B.E. of 284−283 eV is the most dominant peak in the 0:10 sample, inferring lowest defects induced because of only H_3PO_4-treated graphite, which corroborates well with XRD. On addition of H_3PO_4 in small quantity to H_2SO_4 (i.e., 8:2), the percentage of COOH functionalities on GO is nearly unaffected. However, a substantial increase in C═O and C−OH/C−O−C functionalities is observed, confirming the assistance provided by H_3PO_4 in expanding the galleries without compensating the oxidizing potential of $KMnO_4$/acid-mediated oxidation of the graphite surface.

With a further increase in H_3PO_4 content, 5:5, a slight reduction in COOH groups is reflected, but sp^2 domains are still highly etched as dominated by C═O and C−O−C/C−OH groups, which is in good agreement with FTIR. However, with reversal in ratio from 8:2 to 2:8, COOH functionalities doubled with richness of C−C/C−H structures, as shown in Table S3. Surprisingly, a nearly 2.5-fold reduction in C−OH and enhancement in C═O-rich groups is also observed. This

DOI: 10.1021/acsomega.9b00676
ACS Omega 2019, 4, 9407−9418

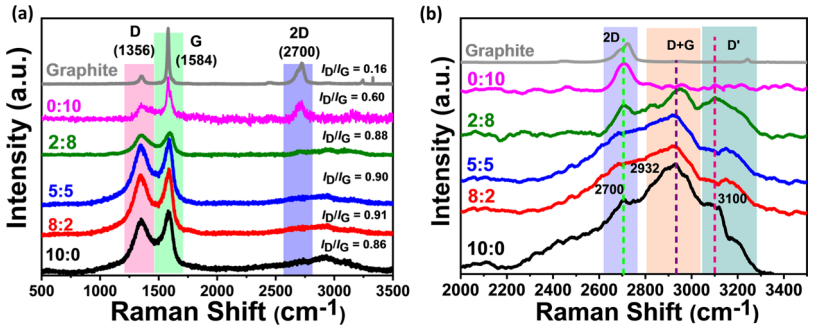

Figure 6. (a) Raman spectra of graphite and synthesized GOs. (b) Zoomed-in image of Raman spectra in the range of 2000−3500 cm^{-1} representing the intensity of 2D, D + G, and D′ bands, suggesting the stacking order of graphite galleries in different oxidation levels.

reduction in C−OH functionalities with increase in H_3PO_4 content is attributed to the conversion of 1,2-diols to the cyclic structures to form C−O−P-linked organophosphates[63] and/or to carbonyl groups from 1,1-diols[64] because of the dehydrating nature of phosphoric acid. Additionally, the water liberated because of conversion of H_3PO_4 to pyrophosphoric acid ($2H_3PO_4 \rightleftharpoons H_4P_2O_7 + H_2O$)[55] may also be responsible for prominence of sp^2 carbon content[65] which also increased with the increase in H_3PO_4 content, that is, for 5:5, 2:8, and 0:10, it increased to 19, 27, and 75%, respectively. Beyond the 5:5 ratio of acid, that is, 2:8 and 0:10, phosphorus (P 2s and P 2p) peaks are evident at B.E. of 191.6 and 134.6 eV, respectively, which corresponds to P as in PO_4^{3-n} of phosphoric acid and organophosphates (Figure S2a).[60,61,66,67] The atomic percentage of P determined as 2 and 13% for 2:8 and 0:10, respectively, supported the observation in FTIR.

The stacked O 1s spectra revealed a broadening of the peak with a significant shift toward lower B.E., with the increase in H_3PO_4 in the intercalant ratio (Figure S2b). This asymmetric development in the shape of the O 1s peak due to different oxidative functionalities suggested the existence and variation of different chemical states of oxygen with single and double bonds with variation in the acid ratio. The fitting of O 1s of 10:0 clearly showed C−O and C═O and/or P═O at 532.8 and 531.3 eV, respectively (Figure S2c).[68] In addition to chemically bound oxygen with carbon on GO, the latter peak also contains a component which is ascribed to the adsorption of phosphoric acid on the GO surface. Despite additional extensive efforts of purification of GOs prepared with 2:8 and 0:10 acid content, P % still remained unchanged, which may be responsible for slightly higher yields, as shown in Table S2. The atomic percentage determined from elemental analysis (Table S4) also supported the presence of S in the samples.

Optical images of GO aqueous dispersions (Figure S3a) clearly showed brown color for all ratios, except 2:8 and 0:10, which is characteristic of existence of highly oxidized GOs. The 2:8 and 0:10 samples showed a brown-gray color, inferring a lower degree of oxygen functionalities. To scrutinize this behavior and also the stability of aqueous dispersion, a time-dependent UV−vis study was performed (Figure S3b). UV−vis spectra of the GOs (Figure S3b) showed absorption due to conjugated carbon double bonds and oxygenated functionalities at ∼227 and ∼300 nm (shoulder), respectively, consistent with the literature.[2] The 0:10 sample showed no absorption features because of its powdery, stacked nature due to the least oxidized surface reconfirming that H_3PO_4 alone is not as equally effective as H_2SO_4 to etch the surface of graphite. The excellent aqueous dispersion stability of synthesized GO from 10:0 to 5:5 is supported by optical images with insignificant changes in absorbance values with time. After 30 days, the absorbance intensity at 300 nm remains unchanged in the 5:5 ratio, consistent with the presence of a higher amount of oxidative functionalities, which is in congruence with XPS and FTIR results. On the contrary, a substantial change in the optical behavior of 2:8 is noticed, with change in absorbance values, which is suggestive of the presence of larger particles with substantially less oxidized areas and/or the existence of residual unoxidized graphite particles.[63] To ascertain whether the settled nanoparticles are unoxidized graphite, they were separated, re-dispersed, and analyzed by UV−vis (inset in Figure S3b) and FTIR (Figure S4). The characteristics are similar to GO particles, confirming heterogeneity in the sample with randomly and sparsely distributed oxo-functionalities with retention of larger graphitic domains, in congruence with XRD and XPS. A noticeable darkening of the aqueous GO dispersion (10:0) is observed after 15 and 30 days, suggesting time-mediated partial re-graphitization in aqueous conditions.

Figure 6 shows the Raman spectra to probe the degree of disorder in synthesized GOs, and the results are compared with graphite.[69] Pristine graphite revealed a weak D band (1356 cm^{-1}) with a sharp and strong G band peak (1584 cm^{-1}) associated with the breathing mode of aromatic rings because of dangling bonds in plane terminations and bond stretching of the sp^2 carbons, respectively. The degree of disorder (intensity ratio, I_D/I_G) is found to increase after oxidation because of introduction of oxidative functionalities in sp^2 domains, consistent with the literature.[56] The I_D/I_G ratio is determined as 0.86 for the 10:0 and 0.6 for 0:10 samples treated with neat H_2SO_4 and H_3PO_4, respectively, confirming that H_2SO_4 assisted in the formation of holes and functional groups at defect sites, whereas H_3PO_4-treated graphite bears relatively more extended conjugated structures.

With the addition of H_3PO_4 in H_2SO_4, the degree of defects increased as indicated by the increase in the I_D/I_G ratio and distance between defects (L_D) (Table S5), suggesting an enhancement in the introduction of defects across the GO because of effective intercalation efficiency and oxidizing capacity of H_3PO_4 in conjunction with H_2SO_4. The calculated average crystallite size (L_a) of the sp^2 domains in the GOs is found to decrease from 148.4 nm in precursor graphite to 22.5, 21.0, 21.3, and 17.0 nm for 10:0, 8:2, 5:5, and 2:8, respectively. This decrease in L_a supported the breaking of crystallites of graphite because of oxidation and formation of defects, disorders, tetrahedral sp^3structures, and crystalline domains, consequently generating amorphous structures in GO. The

DOI: 10.1021/acsomega.9b00676
ACS Omega 2019, 4, 9407−9418

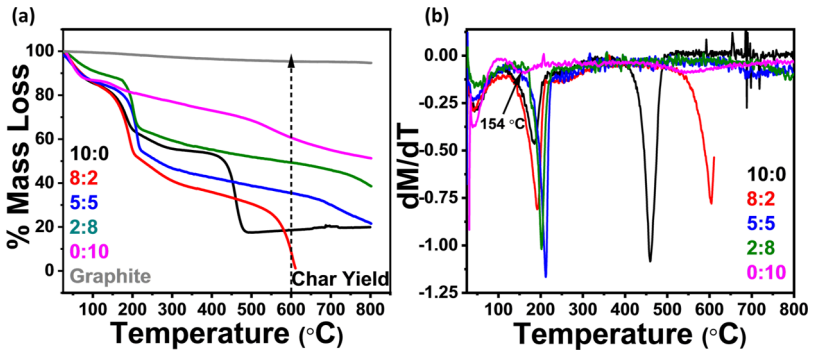

Figure 7. (a) TGA and (b) DTG analyses: graphite and GOs synthesized by varying acid ratios.

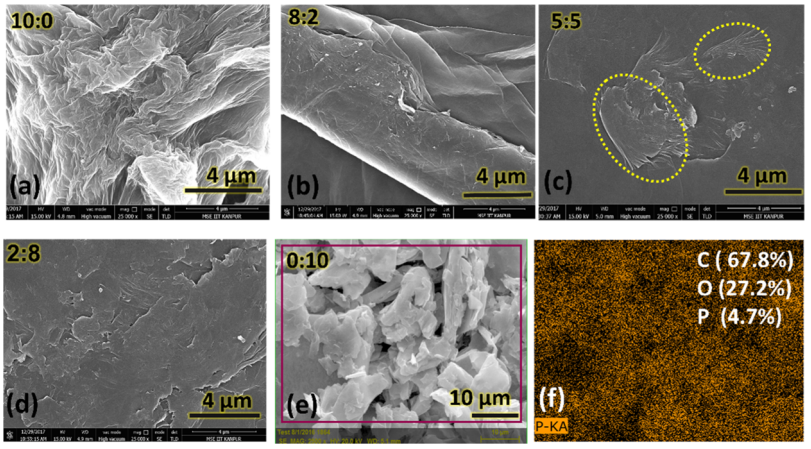

Figure 8. Representative field-emission SEM (a−e) images of GOs; the dotted region in the 5:5 ratio represents the nanostructural leafy domains; (f) EDS mapping of P and % atomic composition in the 0:10 ratio suggesting homogenous distribution of phosphorus in the selected area zone. Scale bar ∼10 μm.

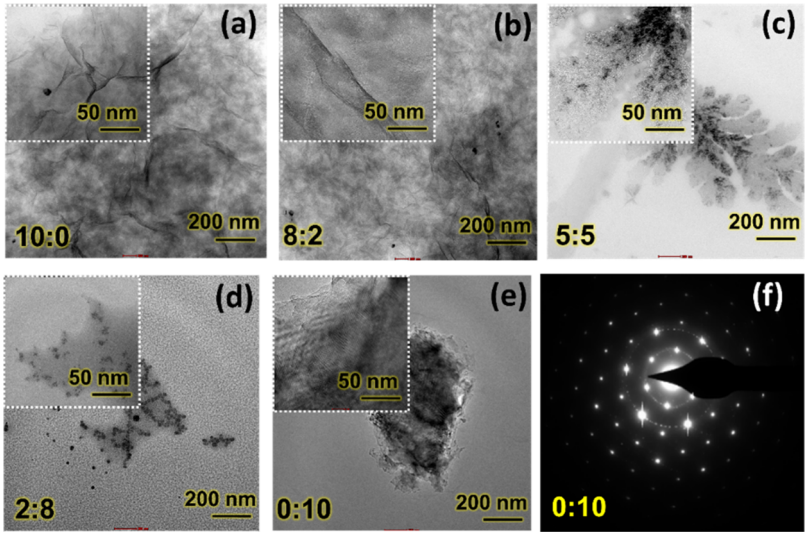

Figure 9. TEM (a−e) images and inset of GO synthesized showing the surface morphology at different resolutions; (f) SAED pattern of the 0:10 sample exhibiting the hexagonal pattern of crystalline domains.

changes in overtone bands, 2D, D + G, and 2G bands (Figure 6b), illustrated the disruption of the graphitic AB stacking order in graphite. In comparison to graphite, overtone bands are apparent, confirming the disordered structure in GOs, with the increasing oxidation level.[54] The I_{2D}/I_G ratio in the case of 0:10 is similar to that of graphite, supporting the existence of stacked nanostructures.

Figure 7 shows the thermogravimetric analysis (TGA) of synthesized GOs, and the respective mass losses are presented in Table S6. Both 10:0 and 8:2 samples showed a three-step decomposition, whereas higher H_3PO_4-treated ratios revealed a two-step mass loss behavior (Figure 7b). The mass loss below 100 °C is due to adsorbed water, that at ∼250 °C is due to loss of labile chemical functionalities such as COOH, C−OH, and

DOI: 10.1021/acsomega.9b00676
ACS Omega 2019, 4, 9407−9418

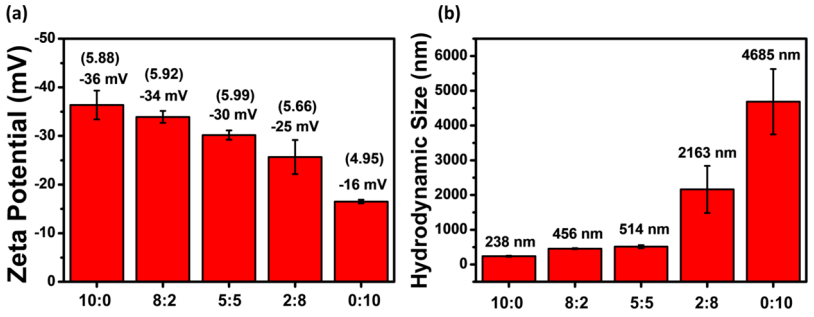

Figure 10. (a) Zeta potential, pH of respective dispersions (in parenthesis), and (b) DLS of different as-obtained GOs in aqueous medium.

epoxides, and a higher mass loss at ≥400 °C is attributed to the degradation of more thermally stable C═C, C═O, and complex functionalities in the graphitic network.[70] The % mass loss observed at 250 °C followed the order of 0:10 < 2:8 < 10:0 < 8:2 ≈ 5:5, confirming the predominance of more labile functionalities in the same fashion, which corroborated well with the XPS (Table S3). TGA data of 0:10 correlated well with the presence of H_3PO_4 and organophosphates structures as determined by XPS and FTIR studies. A mass loss of ∼7% at ∼154 °C (cf. boiling point of H_3PO_4) is indicative of physioadsorbed H_3PO_4 in GO (Figure 6b). Interestingly, a higher char yield (mass left after combustion) is also supportive of the existence of more stable carbon architecture in 0:10 and 2:8 because of a lower degree of oxidation and the presence of phosphorus, as the latter is known to promote carbonization with enhancement in char yield.[71]

The effect of H_3PO_4 incorporation in synthesis revealed a significant variation in the surface morphology of GO as determined by SEM and TEM from Figures 8 and 9, respectively. The SEM image of 10:0-treated GO exhibited excessive wrinkling, whereas 8:2 showed folding and bundling of the sheets. The 5:5 and 2:8 samples revealed a relatively smooth surface morphology. The former ratio showed the presence of nanostructural leafy domains, whereas the latter ratio revealed a layered architecture. In the case of 0:10, aggregation of particles with no regular sheet-type structure is observed. Elemental mapping of 0:10 (Figure 8f) revealed a high percentage of carbon with homogeneous distribution of phosphorus, supporting uniform entrapment of H_3PO_4 and formation of organophosphates across the interlayer spaces within oxo-functionalized graphite sheets, in congruence with FTIR and XPS analyses. The different morphology of GO prepared with variable acid ratios is an indication of different extents of exfoliation, sheet size, and agglomeration of layered structures.

In an analogy, TEM studies (Figure 9) also corroborated well with SEM. The 10:0 sample showed extensive wrinkling of the sheet than the 8:2 sample. In 5:5, leafy domains are clearly visible with folding across, forming the midrib and veins. A heterogeneity in 2:8 is indicative of the difference in degree of oxidation, consistent with UV−vis (Figure S3) and FTIR (Figure S4) results. The 10:0 sample exhibited dense particulates and the existence of graphitic domains as confirmed from selected area electron diffraction (SAED) patterns. The SAED patterns for 10:0, 8:2, and 5:5 showed a typical diffusive ring-like motif because of the merging of diffraction spots across several stacked GOs, indicating the polycrystalline behavior of the samples (Figure S5).[72] The diffused ring diffraction pattern is typical of a disordered structure which is observed in GO, illustrating the disruption of the conjugated structure of graphite due to oxidation. The 2:8 sample showed a little predominance of diffraction spots, which is attributed to the retention of graphene-like lattice substances within the oxidized GO domains (Figure S5d).[72] The existence of such graphitic islands or unoxidized sp^2 domains within the oxidized GO sheets are substantially present as reported previously.[73,74] The 0:10 sample showed a set of sixfold symmetric diffraction points of a typical hexagonal configuration (Figure 9f), which could be attributed to the highest formation of super-lattice-type ordered arrays because of a larger amount of graphitic islands, as also supported by XRD and Raman analysis.

Additionally, AFM images (Figure S6) supported sheet-like morphology and the existence of mono- and few-layered structures in 8:2 and 5:5 samples, respectively. The 2:8 sample showed a very high stacking order of ∼50 nm, which also supported the formation of the layered structure.

The influence of various oxygenated functionalities in GO is evaluated with the help of zeta potential and DLS analysis (Figure 10). Zeta potential (ζ) is necessary for characterizing the electrical properties of interfacial layers in dispersion. The ζ values of synthesized GOs (Figure 10a) in an aqueous dispersion using different ratios of intercalants, that is, 10:0, 8:2, 5:5, 2:8, and 0:10, are measured as −36, −34, −30, −25, and −16 mV, respectively. A value of $\zeta \geq 30$ (negative or positive) is considered to be stable for dispersions because of higher inner-particle electrostatic repulsions originated from ionization of labile groups. A greater ζ value for 10:0, 8:2, and 5:5 implies their higher stability in aqueous dispersion, which is in congruence with UV−vis studies (Figure S2b). The ζ values are attributed to the development of surface charges on nanomaterial because of their interaction with water. The more ionizable groups that are present, such as hydroxyl, phenolic-OH, and −COOH, with higher acid dissociation constants, K_a, are expected to dissociate rapidly to account for higher ζ values of GO. Especially, −COOH and phenolic-OH exhibit relatively easier dissociation because of stabilization of the respective structures by resonance and polar interactions. A decrease in the ζ value is revealed with a decrease in H_2SO_4 in the intercalant ratio, which is a reflection of simultaneous decrease in negatively charged functionalities, as supported by XPS data. In analogy to UV−vis and Raman results, 0:10 showed the lowest ζ, attributable to the least stability of its aqueous dispersion, which is consistent with their lowest density of polar oxo-groups.

In addition, the sheet size, particle size distribution, and colloidal homogeneity of nanoparticles in aqueous media also supported the above observations. The average hydrodynamic sizes of GOs obtained are observed as 238, 456, 534, 2163, and 4865 nm for 10:0, 8:2, 5:5, 2:8, and 0:10 ratio, respectively

DOI: 10.1021/acsomega.9b00676
ACS Omega 2019, 4, 9407−9418

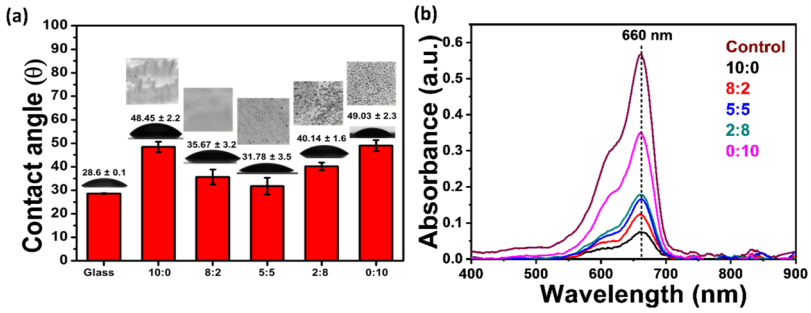

Figure 11. (a) CA and (b) UV−vis spectra of the supernatant obtained from MB-treated GO samples.

(Figure 10b). The smaller size and larger ζ values accounted for a higher colloidal stability and homogeneity for 10:0, 8:2, and 5:5 samples. A larger hydrodynamic size in the latter ratios (2:8 and 0:10) is due to less oxidized graphitic domains along with their relatively larger sheet size, accounting for their moderate to lowest stability in aqueous dispersions.

A qualitative knowledge on the nature of functional groups (ionizable and non-ionizable) (Figure S7) is determined by pH analysis. The acidic −COOH and phenolic −OH groups would react with basic NaOH instantaneously to undergo acid−base neutralization reaction. Whereas carbonyl undergoes nucleophilic addition, epoxide and organophosphates are expected to undergo base-mediated ring opening reaction with NaOH. The control sample (aq. NaOH) showed a pH of 9.7. Base-treated GO samples for 10:0, 8:2, 5:5, 2:8, and 0:10 showed a lowering in pH as a result of consumption of NaOH because of their reaction with GO. A higher consumption of NaOH is observed for 5:5, which is in accordance with the presence of the highest number of base-reactive functional groups. Ideally, 2:8 and 0:10 should reflect the lowest consumption of NaOH because of lower oxygenated functionalities but entrapped H_3PO_4, and the existence of reactive phosphorus structures in these samples accounted for a higher consumption of NaOH.

The nature of functionalities, that is, hydrophilic versus hydrophobic, wettability of the underlying substrate,[75,76] density of coating, and roughness, interplay and affect the CA of water on graphene nanomaterial. To minimize the errors, GO samples are coated at the same concentration on the same substrate with the same volume to pursue the CA measurements. The synthesized GOs (Figure 11a) showed a lower water drop CA than an unsupported graphene (~90°),[77] supporting their hydrophilic nature. The 10:0 and 0:10 showed a higher CA, whereas intermediate ratios exhibited lowering in value, and the least value is observed for 5:5, inferring the highest hydrophilicity and a comparatively smoother surface morphology, consistent with SEM images. The optical images, inset of Figure 11a, of the samples represent similar observations pertaining to roughness and hydrophilic behavior of GOs.[78]

MB (methylthioninium chloride) is a cationic dye, which remained a concern because it is an industrial pollutant in water bodies and demands remedial measures for its removal. Previous reports showed a promising behavior of GO in removal of MB dye.[79] The potential of oxidative functionalities present on GOs along with the π-framework is effective in removal of dye because of both polar and $\pi-\pi$ interactions. To observe the effectiveness of GOs synthesized from different intercalant ratios, aqueous GO dispersions at the same concentrations are used for MB dye removal. The maximum at 660 nm because of MB species is found to decrease with the type of GO used, signifying their potential in MB removal (Figure 11b). The adsorption capacity of the dye on GO is directly proportional to the oxygen functionalities present as they interact effectively with positively charged MB dye via polar interactions. It can be seen from the UV−vis spectra that the adsorption of MB by 10:0 is maximum followed by 8:2 and other ratios. The least adsorption of MB by 0:10 suggested the occurrence of least content of oxygen functionalities on the surface of GO.

4. CONCLUSIONS

In this work, using first-principles simulations and various measurements, we successfully demonstrated the effect of variation in the ratio of acid intercalants, namely, H_2SO_4 and H_3PO_4 in graphite. Understanding the variable intercalation behavior of the two acids, we synthesized GO using various ratios of H_2SO_4 and H_3PO_4 in the presence of $KMnO_4$ to mediate the oxidation of graphite. Both H_2SO_4 and H_3PO_4 are found to control the exfoliation and oxidation of graphite sheets. H_3PO_4 is highly effective in exfoliation of layers of graphite, whereas H_2SO_4 simultaneously controls the extent of oxidation of GO sheets too. Neat H_2SO_4 led to formation of oxygen-rich functionalities, whereas neat H_3PO_4 led to mild oxidation of graphite. The nature and amount of functionalities generated on the GO surface are primarily governed by the ratio of 2. An equivolume ratio of acids led to an enhancement in oxygenated functionalities at the basal plane. The current work suggests that the alteration in the ratio of acids is effective in tailoring the functionality in GOs, thereby advancing their scope for electronic and/or biomedical applications.

■ ASSOCIATED CONTENT

Supporting Information

The Supporting Information is available free of charge on the ACS Publications website at DOI: 10.1021/acsomega.9b00676.

Differential charge density plot and respective O−H bond distances of graphite intercalated with acids, synthesis parameters, XPS spectra for O 1s, survey scan, elemental analysis, elemental analysis, UV−vis, and FTIR spectra, Raman and TGA analysis table, SAED pattern, AFM images, and pH analysis (PDF)

■ AUTHOR INFORMATION

Corresponding Authors

*E-mail: priya.johari@snu.edu.in. Phone: (+91-120) 3819 100 (P.J.).

*E-mail: bimlesh.lochab@snu.edu.in (B.L.).

DOI: 10.1021/acsomega.9b00676
ACS Omega 2019, 4, 9407−9418

ORCID
Bimlesh Lochab: 0000-0002-8434-6513

Author Contributions

N.Y. and V.K. have done the experimental work. D.C. and P.J. have done computer simulations. All the authors have given approval to the final version of the paper.

Notes

The authors declare no competing financial interest.

■ ACKNOWLEDGMENTS

This work was financially supported by Shiv Nadar University. The high-performance computing facility available at the School of Natural Sciences, Shiv Nadar University, was used to perform all the calculations. The work of V.K. was funded through the Opportunities for Undergraduate Research (OUR) scheme.

■ REFERENCES

(1) Dimiev, A. M.; Tour, J. M. Mechanism of graphene oxide formation. *ACS Nano* **2014**, *8*, 3060−3068.
(2) Chen, J.; Li, Y.; Huang, L.; Li, C.; Shi, G. High-yield preparation of graphene oxide from small graphite flakes via an improved Hummers method with a simple purification process. *Carbon* **2015**, *81*, 826−834.
(3) Dong, L.; Chen, Z.; Lin, S.; Wang, K.; Ma, C.; Lu, H. Reactivity-controlled preparation of ultralarge graphene oxide by chemical expansion of graphite. *Chem. Mater.* **2017**, *29*, 564−572.
(4) Liu, Z.; Duan, X.; Zhou, X.; Qian, G.; Zhou, J.; Yuan, W. Controlling and formation mechanism of oxygen-containing groups on graphite oxide. *Ind. Eng. Chem. Res.* **2013**, *53*, 253−258.
(5) Morimoto, N.; Kubo, T.; Nishina, Y. Tailoring the oxygen content of graphite and reduced graphene oxide for specific applications. *Sci. Rep.* **2016**, *6*, 21715.
(6) Peng, L.; Xu, Z.; Liu, Z.; Wei, Y.; Sun, H.; Li, Z.; Zhao, X.; Gao, C. An iron-based green approach to 1-h production of single-layer graphene oxide. *Nat. Commun.* **2015**, *6*, 5716.
(7) Yu, H.; Zhang, B.; Bulin, C.; Li, R.; Xing, R. High-efficient synthesis of graphene oxide based on improved hummers method. *Sci. Rep.* **2016**, *6*, 36143.
(8) Chen, J.; Zhang, Y.; Zhang, M.; Yao, B.; Li, Y.; Huang, L.; Li, C.; Shi, G. Water-enhanced oxidation of graphite to graphene oxide with controlled species of oxygenated groups. *Chem. Sci.* **2016**, *7*, 1874−1881.
(9) Yoo, M. J.; Park, H. B. Effect of hydrogen peroxide on properties of graphene oxide in Hummers method. *Carbon* **2019**, *141*, 515−522.
(10) Pendolino, F.; Armata, N.; Masullo, T.; Cuttitta, A. Temperature influence on the synthesis of pristine graphene oxide and graphite oxide. *Mater. Chem. Phys.* **2015**, *164*, 71−77.
(11) Huang, N. M.; Lim, H.; Chia, C. H.; Yarmo, M. A.; Muhamad, M. Simple room-temperature preparation of high-yield large-area graphene oxide. *Int. J. Nanomed.* **2011**, *6*, 3443.
(12) Skákalová, V.; Kotrusz, P.; Jergel, M.; Susi, T.; Mittelberger, A.; Vretenár, V.; Šiffalovič, P.; Kotakoski, J.; Meyer, J. C.; Hulman, M. Chemical Oxidation of Graphite: Evolution of the Structure and Properties. *J. Phys. Chem. C* **2017**, *122*, 929−935.
(13) Li, C.; Shi, Y.; Chen, X.; He, D.; Shen, L.; Bao, N. Controlled synthesis of graphite oxide: formation process, oxidation kinetics, and optimized conditions. *Chem. Eng. Sci.* **2018**, *176*, 319−328.
(14) Moissette, A.; Fuzellier, H.; Burneau, A.; Dubessy, J.; Guérard, D.; Lelaurain, M. In *Spontaneous Intercalation of Sulfuric Acid into Graphite and Synthesis of a New Graphite-Uranyl Sulfate Compound*; Tchoubar, D., Conard, J., Eds.; Materials Science Forum; Trans Tech Publ: Switzerland, 1992; pp 95−99.
(15) Moissette, A.; Fuzellier, H.; Burneau, A.; Dubessy, J.; Lelaurain, M. Sulfate graphite intercalation compounds: New electrochemical data and spontaneous intercalation. *Carbon* **1995**, *33*, 123−128.
(16) Yosida, Y.; Tanuma, S.; Okabe, K. In situ observation of X-ray diffraction in a synthesis of H_2SO_4-GICs. *Synth. Met.* **1989**, *34*, 341−346.
(17) Metrot, A.; Fischer, J. E. Charge transfer reactions during anodic oxidation of graphite in H_2SO_4. *Synth. Met.* **1981**, *3*, 201−207.
(18) Inagaki, M.; Iwashita, N.; Kouno, E. Potential change with intercalation of sulfuric acid into graphite by chemical oxidation. *Carbon* **1990**, *28*, 49−55.
(19) Schafhaeutl, C. Ueber die Verbindungen des Kohlenstoffes mit Silicium, Eisen und anderen Metallen, welche die verschiedenen Gallungen von Roheisen, Stahl und Schmiedeeisen bilden. *J. Prakt. Chem.* **1840**, *21*, 129−157.
(20) Brodie, B. Note sur un nouveau procédé pour la purification et la désagrégation du graphite. *Ann. Chim. Phys.* **1855**, *45*, 351−353.
(21) Rüdorff, W.; Hofmann, U. Über graphitsalze. *Z. Anorg. Allg. Chem.* **1938**, *238*, 1−50.
(22) Thiele, H. Über die Quellung von Graphit. *Z. Anorg. Allg. Chem.* **1932**, *206*, 407−415.
(23) Dimiev, A. M.; Bachilo, S. M.; Saito, R.; Tour, J. M. Reversible formation of ammonium persulfate/sulfuric acid graphite intercalation compounds and their peculiar Raman spectra. *ACS Nano* **2012**, *6*, 7842−7849.
(24) Kovtyukhova, N. I.; Wang, Y.; Berkdemir, A.; Cruz-Silva, R.; Terrones, M.; Crespi, V. H.; Mallouk, T. E. Non-oxidative intercalation and exfoliation of graphite by Brønsted acids. *Nat. Chem.* **2014**, *6*, 957−963.
(25) Lin, S.; Dong, L.; Zhang, J.; Lu, H. Room-Temperature Intercalation and similar to 1000-Fold Chemical Expansion for Scalable Preparation of High-Quality Graphene. *Chem. Mater.* **2016**, *28*, 2138−2146.
(26) Xu, J.; Dou, Y.; Wei, Z.; Ma, J.; Deng, Y.; Li, Y.; Liu, H.; Dou, S. Recent Progress in Graphite Intercalation Compounds for Rechargeable Metal (Li, Na, K, Al)-Ion Batteries. *Adv. Sci.* **2017**, *4*, 1700146.
(27) Kim, J.; Kim, J.; Song, S.; Zhang, S.; Cha, J.; Kim, K.; Yoon, H.; Jung, Y.; Paik, K.-W.; Jeon, S. Strength dependence of epoxy composites on the average filler size of non-oxidized graphene flake. *Carbon* **2017**, *113*, 379−386.
(28) Kim, J.; Yoon, G.; Kim, J.; Yoon, H.; Baek, J.; Lee, J. H.; Kang, K.; Jeon, S. Extremely large, non-oxidized graphene flakes based on spontaneous solvent insertion into graphite intercalation compound. *Carbon* **2018**, *139*, 309−316.
(29) Morimoto, N.; Suzuki, H.; Takeuchi, Y.; Kawaguchi, S.; Kunisu, M.; Bielawski, C. W.; Nishina, Y. Real-Time, in Situ Monitoring of the Oxidation of Graphite: Lessons Learned. *Chem. Mater.* **2017**, *29*, 2150−2156.
(30) Marcano, D. C.; Kosynkin, D. V.; Berlin, J. M.; Sinitskii, A.; Sun, Z.; Slesarev, A.; Alemany, L. B.; Lu, W.; Tour, J. M. Improved synthesis of graphene oxide. *ACS Nano* **2010**, *4*, 4806−4814.
(31) Yadav, N.; Dubey, A.; Shukla, S.; Saini, C. P.; Gupta, G.; Priyadarshini, R.; Lochab, B. Graphene Oxide-Coated Surface: Inhibition of bacterial biofilm formation due to specific surface−interface interactions. *ACS Omega* **2017**, *2*, 3070−3082.
(32) Becerra-Paniagua, D. K.; Sotelo-Lerma, M.; Hu, H. Highly oxidized and exfoliated graphene using a modified Tour approach. *J. Mater. Sci.: Mater. Electron.* **2019**, *30*, 3973−3983.
(33) Park, W. K.; Yoon, Y.; Kim, S.; Choi, S. Y.; Yoo, S.; Do, Y.; Jung, S.; Yoon, D. H.; Park, H.; Yang, W. S. Toward Green Synthesis of Graphene Oxide Using Recycled Sulfuric Acid via Couette−Taylor Flow. *ACS Omega* **2017**, *2*, 186−192.
(34) Kumar, N.; Srivastava, V. C. Simple Synthesis of Large Graphene Oxide Sheets via Electrochemical Method Coupled with Oxidation Process. *ACS Omega* **2018**, *3*, 10233−10242.
(35) Hérold, A. Synthesis of Graphite Intercalation Compounds, Chemical Physics of Intercalation. *NATO ASI Ser., Ser. B* **1987**, *17*, 1.
(36) Koch, K. R. Oxidation by Mn207: An impressive demonstration of the powerful oxidizing property of dimanganeseheptoxide. *J. Chem. Educ.* **1982**, *59*, 973.
(37) Lucchese, M. M.; Stavale, F.; Ferreira, E. H. M.; Vilani, C.; Moutinho, M. V. O.; Capaz, R. B.; Achete, C. A.; Jorio, A. Quantifying

DOI: 10.1021/acsomega.9b00676
ACS Omega 2019, 4, 9407−9418

ion-induced defects and Raman relaxation length in graphene. *Carbon* **2010**, *48*, 1592−1597.
(38) Cançado, L. G.; Takai, K.; Enoki, T.; Endo, M.; Kim, Y. A.; Mizusaki, H.; Jorio, A.; Coelho, L. N.; Magalhães-Paniago, R.; Pimenta, M. A. General equation for the determination of the crystallite size L a of nanographite by Raman spectroscopy. *Appl. Phys. Lett.* **2006**, *88*, 163106−163108.
(39) Kresse, G.; Furthmüller, J. Efficient iterative schemes for ab initio total-energy calculations using a plane-wave basis set. *Phys. Rev. B: Condens. Matter Mater. Phys.* **1996**, *54*, 11169−11186.
(40) Kresse, G.; Furthmüller, J. Efficiency of ab-initio total energy calculations for metals and semiconductors using a plane-wave basis set. *Comput. Mater. Sci.* **1996**, *6*, 15−50.
(41) Kresse, G.; Joubert, D. From ultrasoft pseudopotentials to the projector augmented-wave method. *Phys. Rev. B: Condens. Matter Mater. Phys.* **1999**, *59*, 1758−1775.
(42) Klimeš, J.; Bowler, D. R.; Michaelides, A. Chemical accuracy for the van der Waals density functional. *J. Phys.: Condens. Matter* **2010**, *22*, 022201.
(43) Klimeš, J.; Bowler, D. R.; Michaelides, A. van der Waals density functionals applied to solids. *Phys. Rev. B: Condens. Matter Mater. Phys.* **2011**, *83*, 195131.
(44) Dion, M.; Rydberg, H.; Schröder, E.; Langreth, D. C.; Lundqvist, B. I. van der Waals density functional for general geometries. *Phys. Rev. Lett.* **2004**, *92*, 246401.
(45) Román-Pérez, G.; Soler, J. M. Efficient implementation of a van der Waals density functional: application to double-wall carbon nanotubes. *Phys. Rev. Lett.* **2009**, *103*, 096102.
(46) Dimiev, A. M.; Ceriotti, G.; Behabtu, N.; Zakhidov, D.; Pasquali, M.; Saito, R.; Tour, J. M. Direct real-time monitoring of stage transitions in graphite intercalation compounds. *ACS Nano* **2013**, *7*, 2773−2780.
(47) Eigler, S.; Enzelberger-Heim, M.; Grimm, S.; Hofmann, P.; Kroener, W.; Geworski, A.; Dotzer, C.; Röckert, M.; Xiao, J.; Papp, C.; Lytken, O.; Steinrück, H.-P.; Müller, P.; Hirsch, A. Wet chemical synthesis of graphene. *Adv. Mater.* **2013**, *25*, 3583−3587.
(48) Eigler, S. Graphite sulphate−a precursor to graphene. *Chem. Commun.* **2015**, *51*, 3162−3165.
(49) Seiler, S.; Halbig, C. E.; Grote, F.; Rietsch, P.; Börrnert, F.; Kaiser, U.; Meyer, B.; Eigler, S. Effect of friction on oxidative graphite intercalation and high-quality graphene formation. *Nat. Commun.* **2018**, *9*, 836−844.
(50) Eklund, P. C.; Olk, C. H.; Holler, F. J.; Spolar, J. G.; Arakawa, E. T. Raman scattering study of the staging kinetics in the c-face skin of pyrolytic graphite-H_2SO_4. *J. Mater. Res.* **1986**, *1*, 361−367.
(51) Yang, L.; Zhang, R.; Liu, B.; Wang, J.; Wang, S.; Han, M.-Y.; Zhang, Z. Π-conjugated carbon radicals at graphene oxide to initiate ultrastrong chemiluminescence. *Angew. Chem.* **2014**, *53*, 10109−10113.
(52) Kang, J. H.; Kim, T.; Choi, J.; Park, J.; Kim, Y. S.; Chang, M. S.; Jung, H.; Park, K. T.; Yang, S. J.; Park, C. R. Hidden second oxidation step of Hummers method. *Chem. Mater.* **2016**, *28*, 756−764.
(53) Park, J.; Kim, Y. S.; Sung, S. J.; Kim, T.; Park, C. R. Highly dispersible edge-selectively oxidized graphene with improved electrical performance. *Nanoscale* **2017**, *9*, 1699−1708.
(54) Wang, H.; Hu, Y. H. Effect of oxygen content on structures of graphite oxides. *Ind. Eng. Chem. Res.* **2011**, *50*, 6132−6137.
(55) Kutty, T. R. N.; Vasudeva Murthy, A. R. The instability of permanganate in orthophosphoric acid. *Z. Anorg. Allg. Chem.* **1970**, *379*, 218−224.
(56) Krishnamoorthy, K.; Veerapandian, M.; Yun, K.; Kim, S.-J. The chemical and structural analysis of graphene oxide with different degrees of oxidation. *Carbon* **2013**, *53*, 38−49.
(57) Acik, M.; Lee, G.; Mattevi, C.; Chhowalla, M.; Cho, K.; Chabal, Y. J. Unusual infrared-absorption mechanism in thermally reduced graphene oxide. *Nat. Mater.* **2010**, *9*, 840−845.
(58) Si, Y.; Samulski, E. T. Synthesis of water soluble graphene. *Nano Lett.* **2008**, *8*, 1679−1682.
(59) Stankovich, S.; Piner, R. D.; Nguyen, S. T.; Ruoff, R. S. Synthesis and exfoliation of isocyanate-treated graphene oxide nanoplatelets. *Carbon* **2006**, *44*, 3342−3347.
(60) Rudolph, W. W. Raman-and infrared-spectroscopic investigations of dilute aqueous phosphoric acid solutions. *Dalton Trans.* **2010**, *39*, 9642−9653.
(61) Fleming, I.; Williams, D. H. *Spectroscopic Methods in Organic Chemistry*; Wiley, 1966.
(62) Chen, J.; Li, Y.; Huang, L.; Jia, N.; Li, C.; Shi, G. Size Fractionation of Graphene Oxide Sheets via Filtration through Track-Etched Membranes. *Adv. Mater.* **2015**, *27*, 3654−3660.
(63) Higginbotham, A. L.; Kosynkin, D. V.; Sinitskii, A.; Sun, Z.; Tour, J. M. Lower-defect graphene oxide nanoribbons from multiwalled carbon nanotubes. *ACS Nano* **2010**, *4*, 2059−2069.
(64) Dimiev, A.; Kosynkin, D. V.; Alemany, L. B.; Chaguine, P.; Tour, J. M. Pristine graphite oxide. *J. Am. Chem. Soc.* **2012**, *134*, 2815−2822.
(65) Abrahami, S. T.; Hauffman, T.; de Kok, J. M. M.; Mol, J. M. C.; Terryn, H. XPS analysis of the surface chemistry and interfacial bonding of barrier-type Cr (VI)-free anodic oxides. *J. Phys. Chem. C* **2015**, *119*, 19967−19975.
(66) Rotole, J. A.; Sherwood, P. M. A. Aluminum phosphate by XPS. *Surf. Sci. Spectra* **1998**, *5*, 60−66.
(67) Kannan, A. G.; Choudhury, N. R.; Dutta, N. K. Synthesis and characterization of methacrylate phospho-silicate hybrid for thin film applications. *Polymer* **2007**, *48*, 7078−7086.
(68) Sherwood, P. M. A. Data analysis in X-ray photoelectron spectroscopy. In *Practical Surface Analysis*; Briggs, D., Seah, M. P., Eds.; Wiley: Chichester, 1990; Vol. *1*.
(69) Pimenta, M. A.; Dresselhaus, G.; Dresselhaus, M. S.; Cançado, L. G.; Jorio, A.; Saito, R. Studying disorder in graphite-based systems by Raman spectroscopy. *Phys. Chem. Chem. Phys.* **2007**, *9*, 1276−1290.
(70) Lavin-Lopez, M. d. P.; Romero, A.; Garrido, J.; Sanchez-Silva, L.; Valverde, J. L. Influence of different improved hummers method modifications on the characteristics of graphite oxide in order to make a more easily scalable method. *Ind. Eng. Chem. Res.* **2016**, *55*, 12836−12847.
(71) Cao, Y.; Wang, X.-L.; Zhang, W.-Q.; Yin, X.-W.; Shi, Y.-Q.; Wang, Y.-Z. Bi-DOPO structure flame retardants with or without reactive group: their effects on thermal stability and flammability of unsaturated polyester. *Ind. Eng. Chem. Res.* **2017**, *56*, 5913−5924.
(72) Wilson, N. R.; Pandey, P. A.; Beanland, R.; Young, R. J.; Kinloch, I. A.; Gong, L.; Liu, Z.; Suenaga, K.; Rourke, J. P.; York, S. J.; Sloan, J. Graphene oxide: structural analysis and application as a highly transparent support for electron microscopy. *ACS Nano* **2009**, *3*, 2547−2556.
(73) de La Cruz, F. A.; Cowley, J. M. Structure of graphitic oxide. *Nature* **1962**, *196*, 468−469.
(74) De La Cruz, F. A.; Cowley, J. M. An electron diffraction study of graphitic oxide. *Acta Crystallogr.* **1963**, *16*, 531−534.
(75) Shih, C.-J.; Strano, M. S.; Blankschtein, D. Wetting translucency of graphene. *Nat. Mater.* **2013**, *12*, 866−869.
(76) Rafiee, J.; Mi, X.; Gullapalli, H.; Thomas, A. V.; Yavari, F.; Shi, Y.; Ajayan, P. M.; Koratkar, N. A. Wetting transparency of graphene. *Nat. Mater.* **2012**, *11*, 217−222.
(77) Andrews, J. E.; Sinha, S.; Chung, P. W.; Das, S. Wetting dynamics of a water nanodrop on graphene. *Phys. Chem. Chem. Phys.* **2016**, *18*, 23482−23493.
(78) Andrews, J. E.; Wang, Y.; Sinha, S.; Chung, P. W.; Das, S. Roughness-induced chemical heterogeneity leads to large hydrophobicity in wetting-translucent nanostructures. *J. Phys. Chem. C* **2017**, *121*, 10010−10017.
(79) Yang, S.-T.; Chen, S.; Chang, Y.; Cao, A.; Liu, Y.; Wang, H. Removal of methylene blue from aqueous solution by graphene oxide. *J. Colloid Interface Sci.* **2011**, *359*, 24−29.

DOI: 10.1021/acsomega.9b00676
ACS Omega 2019, 4, 9407−9418